Progress In Electromagnetics Research Letters, Vol. 106, 21–29, 2022

Compact and Broadband Dual-Mode Dipole Antenna

Rajbala Solanki*

Abstract—A compact and broadband stub-loaded dual-mode dipole antenna is proposed. In this paper, the first- and third-order modes are combined to achieve broadband frequency response. To do so, the third-order mode is compressed close to the first-order mode by loading two pairs of identical stubs at an optimal distance from the dipole-centre. Stubs are symmetrically loaded to both the arms of the dipole. Stub parameters such as length, width, and location play a critical role in decreasing the third-order mode frequency. Therefore, a parametric analysis is also carried out to see the effects of variation in the stub parameters. The proposed antenna is fabricated, and measurements are performed to verify the simulation results. A good agreement between the simulated and measured results is obtained.

1. INTRODUCTION

The need of high-speed data transmission with low latency in modern portable wireless communication systems has popularized compact and wideband antennas. Various communication systems may require omnidirectional radiation. This need can be fulfilled by dipole antennas. Although conventional thin wire dipole antennas have narrow bandwidth, various techniques have been reported in the literature to make the dipole antennas broadband [1–28]. To achieve wide bandwidth, differently shaped dipole antennas have been designed such as rectangular arms [1], circular arms [2], U-shaped bow-tie [3–5], half bow-tie [6], Koch-fractal bow-tie [7], conical bow-tie [8], and angled dipoles [9]. The disadvantages of these antennas are: pattern variation over the band, high cross-pols, and large electrical area. Another technique to broaden the bandwidth is the creation of multiple resonances nearby. Multiple resonances can be created by parasitic resonators such as stripline resonator [10], split-ring resonator [11], combination of stripline and split-ring resonators [12], loop resonator [13], combination of stripline and loop resonators [14], sequentially-rotated parasitic-elements [15], pentagonal and trapezoidal parasitic elements [16], fan shaped meandered dipole [17], a shorted patch [18], and array of near-field resonant-parasitic (NFRP) elements [19]. Multiple resonances can also be created by introducing stubs [20], slots [21], their combinations [22], and loading lumped or distributed passive elements [23]. Generally, loading parasitic elements close to the dipole antenna affects the radiation pattern and increases the overall size of the antenna.

Recently, a lot of work/research is going on to achieve wide bandwidth using mode compression technique. In this technique, more than one mode of an antenna are compressed and combined together which results in a wide bandwidth. Dipole antennas are loaded with shorting post/vias [24], lumped elements [25], and differently shaped stubs [26–28] to obtain broadband response. In [24], a via-loaded microstrip magnetic dipole antenna is realized, and two sets of shorting vias are loaded at the voltage null points of the half-TE_{310} mode. This increases the resonance frequency of the half-TE_{110} mode. In [25], a dual-mode dipole antenna is realized by loading two lumped or distributed capacitors at the points where current nulls of the third-order mode occur. With the two capacitive loadings, the

Received 1 June 2022, Accepted 3 August 2022, Scheduled 18 August 2022
* Corresponding author: Rajbala Solanki (rajbala21@gmail.com).
The author is with the Department of Electrical Engineering, Indian Institute of Technology Bombay, Mumbai, India.

fundamental frequency increases towards the third-order mode frequency, and the combination of these two modes results in a bandwidth of 51.4%. However, the electrical size of the antenna becomes larger ($0.815\lambda_L \times 0.123\lambda_L$) due to the increase in fundamental frequency. The fifth-order mode is compressed close to the third-order mode by loading stripline stubs [26] and bent-stubs [27]. Bandwidths of 8.7% and 22.2% are achieved with an electrical size of $0.99\lambda_L \times 0.792\lambda_L$ and $0.978\lambda_L \times 0.978\lambda_L$ in [26] and [27], respectively. These two antennas suffer from high sidelobe levels (SLLs) due to the higher order mode dipoles. In [28], third-order mode is compressed towards the fundamental mode by loading an electrically small loop resonator, and 27.8% bandwidth is obtained with an antenna size of $0.392\lambda_L \times 0.147\lambda_L$.

In this paper, third-order mode is compressed towards the fundamental mode by loading two pairs of stubs. The stub length, width, and position are the critical parameters for the frequency shifting of the third-order mode. A prototype of the proposed antenna is fabricated. Experiments are performed to validate the simulated results. The proposed antenna has a compact size of $0.35\lambda_L \times 0.09\lambda_L$, and it provides 66.2% bandwidth. The radiation pattern is stable over the band with 3.1 dBi peak gain.

2. ANTENNA DESIGN AND ANALYSIS

2.1. Antenna Design

Figure 1 presents the geometry of the proposed dual-mode dipole antenna. The antenna is designed on a substrate with dielectric constant $\varepsilon_r = 2.55$, thickness $h = 1.524$ mm, and loss tangent $\tan\delta = 0.018$. The two identical arms of the dipole are printed on the top and bottom sides of the substrate. The dipole-arms are symmetric about the x-axis (i.e., along dipole-width). The width of the dipole-arms is linearly tapered from W_{d1} (at L_{d1} distance from the dipole-centre) to W_d (at L_{d2} distance from the dipole-centre). This width-tapering is done so that stubs can be loaded without affecting the overall size of the antenna. Each dipole arm is loaded with two identical rectangular stubs at L_{d2} distance from the dipole-centre. The length of the stubs is selected such that there is some overlap area L_{ov} between the top and bottom stubs. A dipole antenna requires balanced feed which is provided through a balun. Here, balun is realized through tapered microstrip line to stripline transition [31] as shown in Figure 1(b). The balun is designed on a thinner substrate with $h_1 = 0.762$ mm and $\varepsilon_r = 2.55$. The dimensions of the

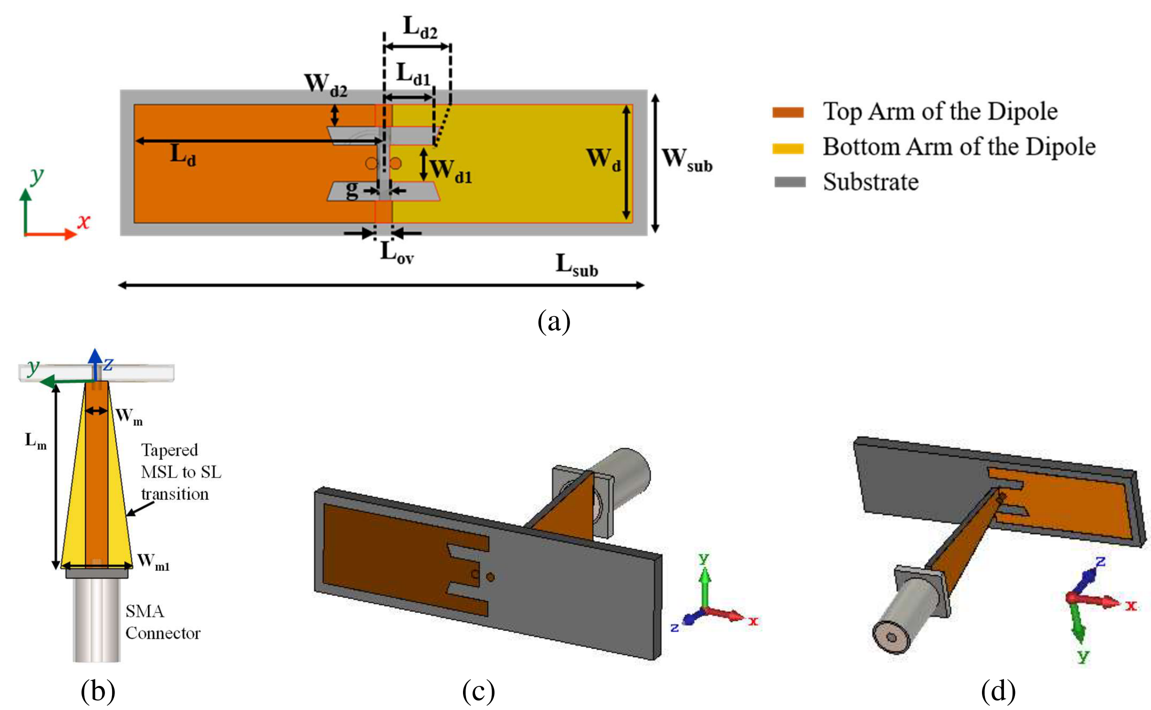

Figure 1. (a) Proposed antenna, and (b) balun geometries with their parameters, (c) front 3D, and (d) back 3D views.

Table 1. Antenna and balun parameters.

L_{sub}	35 mm	L_d	17 mm	L_{d1}	3 mm
W_{sub}	9 mm	W_d	8 mm	W_{d1}	2.5 mm
L_{d2}	4 mm	W_{d2}	1.5 mm	$g = h_1 + 2t$	0.832 mm
L_{ov}	1.2 mm				
L_m	20 mm	W_m	2.2 mm	W_{m1}	7 mm

t is the thickness of the annealed copper layer.

antenna and balun are listed in Table 1. The antenna is designed on CST STUDIO SUITE 2017, and simulations are done using Time-Domain solver in which both finite integration technique (FIT) and transmission line matrix (TLM) implementations are included in a single package [32].

2.2. Development Stages

The proposed antenna is designed in two stages as displayed in Figure 2(a). Simulated $|S_{11}|$ for these two stages are presented in Figure 2(b). In Stage 1, a tapered-width dipole antenna is designed so that stubs can be added without increasing the overall size of the antenna. The first- and third-order mode frequencies for Stage 1 are 3.3 GHz and 10.0 GHz, respectively. To achieve broad bandwidth, the third-order mode is compressed close to the first-order mode. To realize this, path length for the third-order mode is increased by loading stubs at the current null points of the third-order mode. So, in Stage 2, each arm of the dipole is loaded with two identical stubs which are placed symmetrically along the dipole width. The first-order mode frequency is not affected significantly (and to be precise, it increases slightly to 3.4 GHz) whereas the third-order mode frequency decreases to 5.15 GHz. Therefore, the combination of first- and third-order modes results in a wide bandwidth of approx. 64% in Stage 2 from a 19% bandwidth in Stage 1.

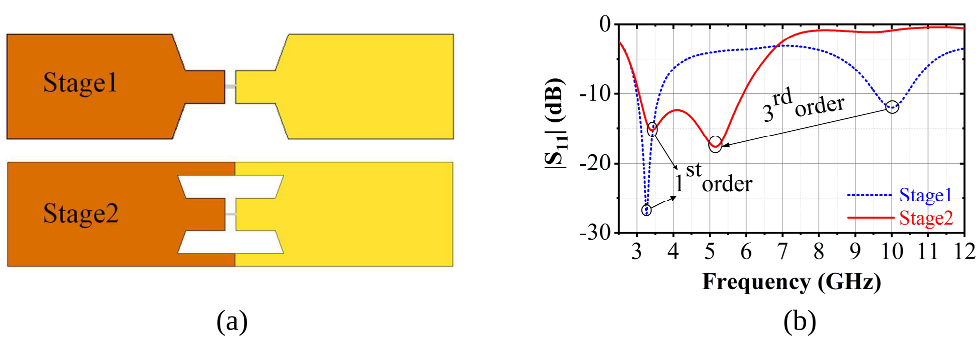

Figure 2. (a) Different stages of the antenna and their simulated (b) reflection coefficient (dB).

2.3. Parametric Analysis

A parametric analysis is presented here to show the effects of the stub parameters. Initially, overlap length L_{ov} is increased from 0.2 mm to 1.2 mm by keeping other parameters fixed to the values given in Table 1. Figure 3 presents the simulated $|S_{11}|$ and input impedance for three values of L_{ov}. As overlap length increases, the third-order mode frequency decreases whereas the first-order mode frequency remains approximately the same. This is also indicated in input reactance curve. The overlap length $L_{ov} = 0.7$ mm provides more bandwidth. However, to take sufficient margin for fabrication and measurement tolerances, $L_{ov} = 1.2$ mm is chosen for the final antenna design. Next, stub width W_{d2} is increased from 0.5 mm to 1.5 mm. The simulated results for $W_{d2} = 0.5$ mm, 1.0 mm, and 1.5 mm are presented in Figure 4. As the stub width increases, the first-order mode frequency is not affected significantly whereas the third-order mode frequency decreases by a large amount. It is validated by

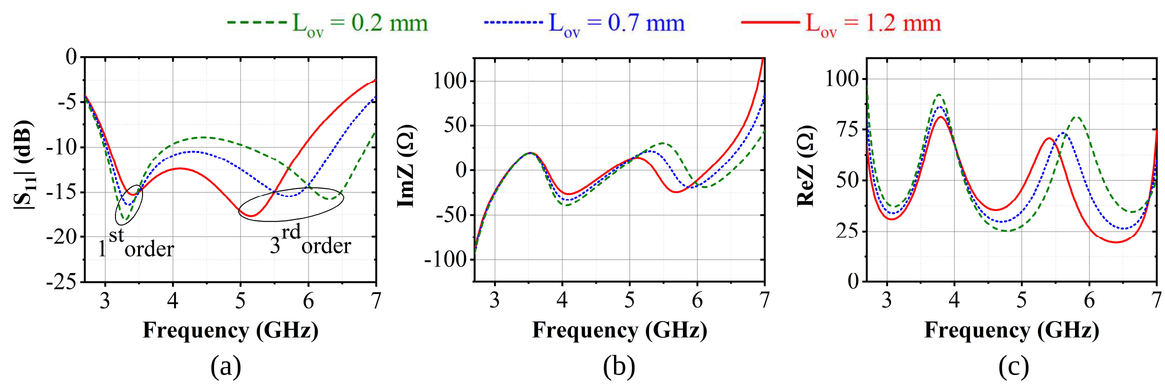

Figure 3. Variation in overlap length L_{ov}: (a) $|S_{11}|$, (b) input reactance and (c) input resistance vs frequency plots.

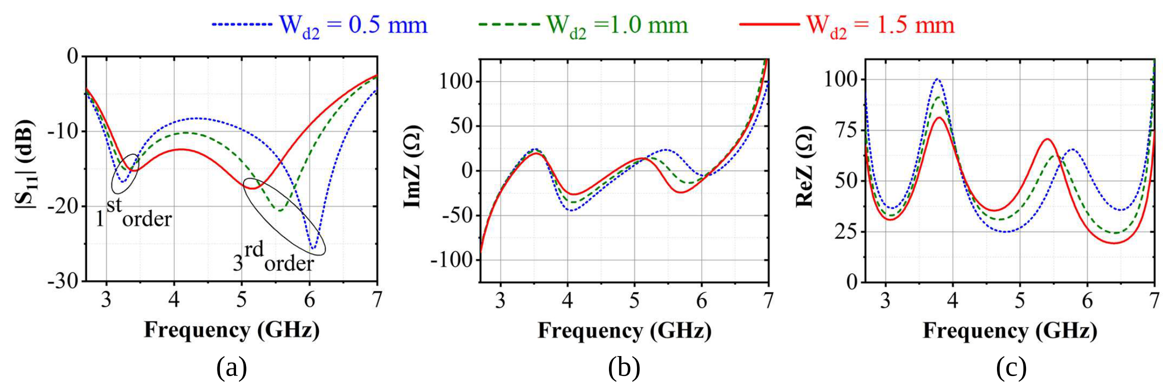

Figure 4. Variation in stub width W_{d2}: (a) $|S_{11}|$, (b) input reactance and (c) input resistance vs frequency plots.

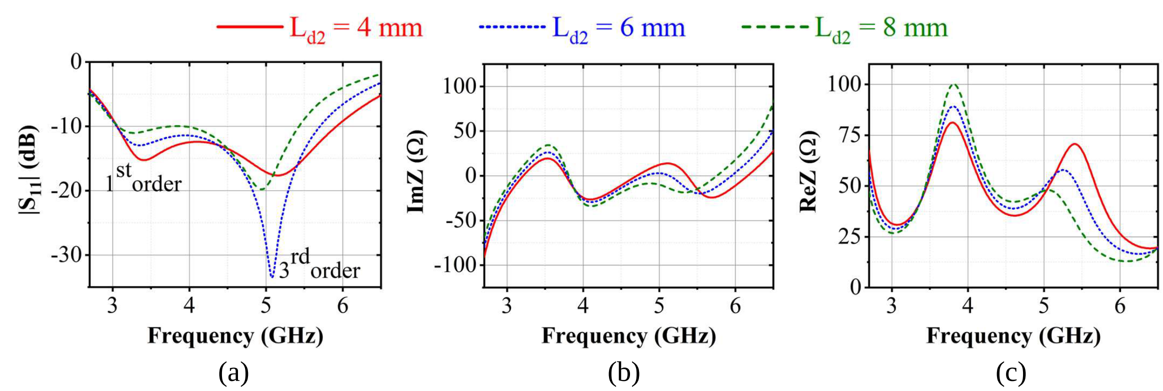

Figure 5. Variation in stub location L_{d2}: (a) $|S_{11}|$, (b) input reactance and (c) input resistance vs frequency plots.

the reactance vs frequency plot shown in Figure 4(b). The stub width $W_{d2} = 1.5\,\text{mm}$ is chosen for the final antenna design. Next, stub position is varied by changing L_{d2} and keeping the stub width $W_{d2} = 1.5\,\text{mm}$ and overlap length $L_{ov} = 1.2\,\text{mm}$. L_{d2} is increased from 4 mm to 8 mm. Variation in the stub position affects both first- and third-order mode frequencies as shown in Figure 5. However, the effects on the first-order mode are less than the third-order mode. As the stubs move away from the centre of the dipole, both the first- and third-order mode frequencies decrease as shown in Figures 5(a) and (b). The stub position $L_{d2} = 4\,\text{mm}$ is selected for the final antenna design.

2.4. Current Distribution and Efficiency

Figure 6 presents the surface currents at 3.25 GHz and 5.5 GHz. As seen from Figure 6(a), there is a half sinusoidal variation of surface currents on the dipole. Therefore, first-order mode is dominant at 3.25 GHz. There is three half sinusoidal variation of surface currents along the dipole length at 5.5 GHz. Therefore, at 5.5 GHz third-order mode is dominant. Another thing to notice from Figure 6(b) is that the maximum surface currents are on the central part of the dipole and on the stubs. That means maximum surface currents for the central half-sinusoid and smaller surface currents for the two outer half-sinusoids. This realizes amplitude tapering along the dipole length which improves the radiation pattern of the antenna at the third-order mode (i.e., reduced sidelobes at higher order modes). Figure 7 presents the radiation and total efficiencies of the proposed antenna. As seen from this figure the radiation and total efficiencies are better than 96% and 87%, respectively for the entire impedance bandwidth. It means that the proposed antenna radiates effectively for the obtained impedance bandwidth.

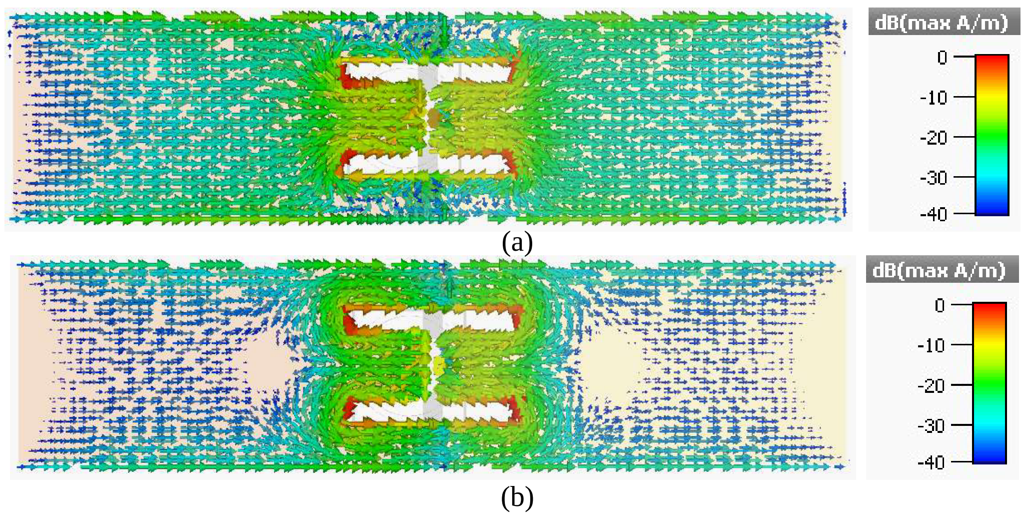

Figure 6. Current distribution at: (a) 3.25 GHz, and (b) 5.5 GHz.

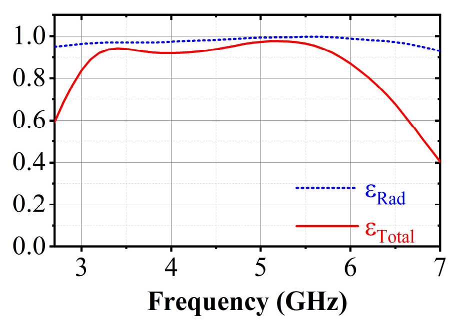

Figure 7. Efficiency of the antenna.

3. MEASURED RESULTS

After going through the parametric analysis, the proposed dual-mode dipole antenna is optimized by taking sufficient margin for various tolerances including fabrication, assembly, material, measurements tolerances, etc. The fabricated prototype is displayed in Figure 8(a). The dipole antenna is fed using a balun realized through a tapered microstrip to stripline transition. A 50 Ω SMA-Male connector is connected to the balun. $|S_{11}|$ is measured using a vector network analyzer and presented in Figure 8(b) along with the simulated $|S_{11}|$. The simulated and measured bandwidths for $|S_{11}| \leq -10$ dB are from

3.05 GHz to 5.92 GHz and from 2.97 GHz to 5.91 GHz, respectively. The electrical size of the antenna is $0.35\lambda_L \times 0.09\lambda_L$ at the lowest frequency of operation. The measured peak gain is approximately 3.1 dBi as shown in Figure 8(c). Figure 9 presents the normalized radiation patterns of the antenna at 3.25 GHz and 5.5 GHz. The E- and H-plane patterns are figure-of-eight and omnidirectional, respectively at both the modes. The cross-pols are less than -16 dB in both E- and H-planes. The radiation pattern is relatively stable over the band.

4. COMPARISON WITH LITERATURE

The proposed dual-mode dipole antenna is compared with the literature, and comparisons are tabulated in Table 2. Comparisons are done in terms of achieved bandwidth, gain and cross-pols, electrical size and figure-of-merit (FoM) of antennas. As discussed in [29, 30], the FoM of antennas can be defined as the ratio of gain bandwidth product and the electrical size. In [24], the obtained gain is the highest, but FoM is smaller due to larger electrical size and smaller BW. The electrical size of the antennas in [11, 19, 28] is comparable to the proposed antenna, but the FoM is smaller because of smaller bandwidths. In [25–27],

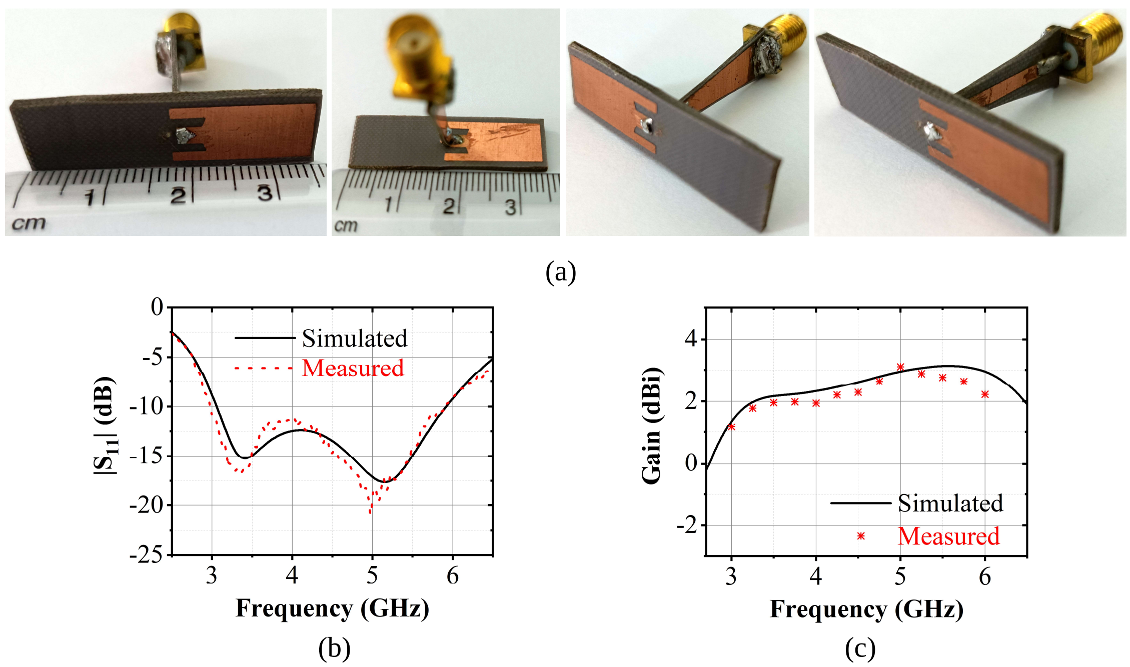

Figure 8. (a) Different views of the fabricated prototype, (b) $|S_{11}|$ and (c) gain plots.

Table 2. Comparison.

Ref.-Year	Size ($\lambda_L \times \lambda_L$)	BW (GHz)	BW (%)	Gain (dBi)	X-pols (dB)	FoM
[11]-2017	0.49×0.25	1.85–2.9	44.2	2.0–4.6	< -8	1041
[19]-2020	0.39×0.15	2.05–2.37	14.4	1.4–1.6	< -14	340
[24]-2019	2.03×0.63	9.81–10.74	9.1	7.2–10.2	< -20	75
[25]-2020	0.82×0.12	1.88–3.18	51.4	2.0–4.0	< -10	1312
[26]-2019	0.99×0.79	3.3–3.6	8.7	3.0–5.0	< -15	35
[27]-2021	0.98×0.98	3.26–4.075	22.2	4.4–6.0	< -15	92
[28]-2020	0.39×0.15	2.94–3.89	27.8	1.8–2.1	< -10	771
Proposed Work	0.35×0.09	2.97–5.91	66.2	1.3–3.1	< -16	4291

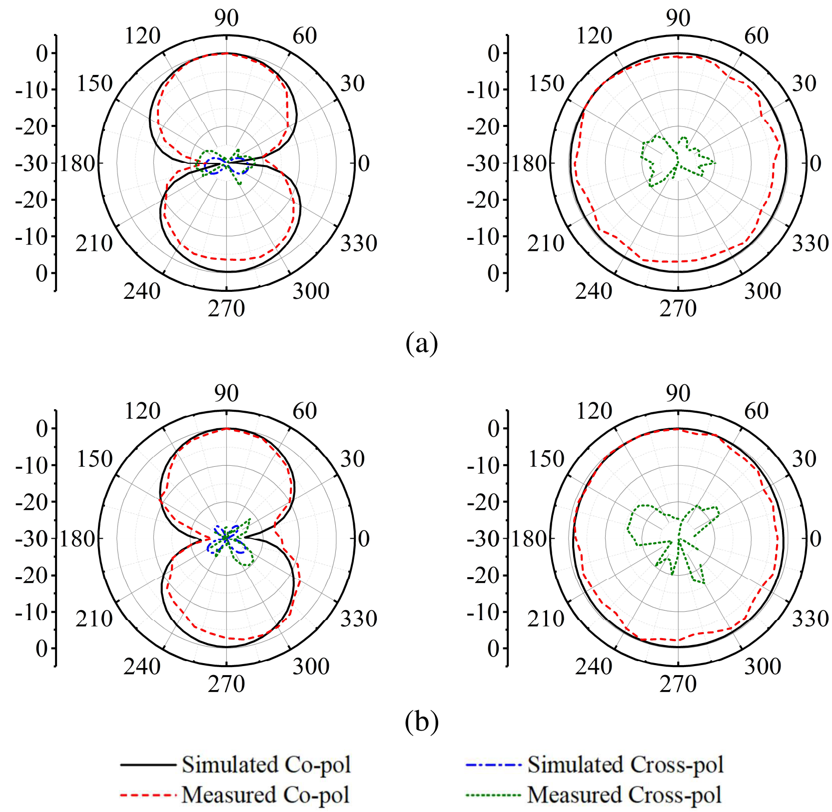

Figure 9. Normalized radiation-patterns at (a) 3.25 GHz, and (b) 5.5 GHz.

the antenna sizes are very large as compared to the proposed antenna, and bandwidth is also smaller which results in smaller FoM than the proposed antenna. The proposed antenna has a smaller electrical size ($= 0.35\lambda_L \times 0.09\lambda_L$) and provides larger FoM bandwidth ($= 66.2\%$) and a decent peak gain of 3.1 dBi. This results in a better FoM than others in the literature.

5. CONCLUSION

A compact stub loaded dual-mode dipole antenna is proposed for broadband frequency response and stable omnidirectional radiation. Wide bandwidth is achieved by compressing and combining the third-order mode with the first-order mode. It is realized by loading two pairs of stubs at the approx. current null points of the third-order mode. The stub parameters play a critical role in deciding the compressed/shifted third-order mode frequency. A prototype of the antenna is fabricated, and measurements validate the simulated results. The overall electrical size of the antenna is $0.35\lambda_L \times 0.09\lambda_L$. A 66.2% bandwidth, 3.1 dBi peak gain, and stable radiation pattern are obtained. The proposed antenna provides better results in a smaller electrical size than the literature. Therefore, it can be a good choice for omnidirectional radiation in sub-6 GHz frequency band.

REFERENCES

1. Mani, M., R. Moolat, K. Vasudevan, and P. Mohanan, "Harmonic suppressed compact stepped impedance uniplanar dipole antenna for WLAN applications," *Progress In Electromagnetics Research Letters*, Vol. 79, 45–50, 2018.
2. Gunaram, J. K. D. and V. Sharma, "Dual band circular polarized printed dipole antenna for S and C band wireless applications," *Progress In Electromagnetics Research C*, Vol. 105, 129–146, 2020.

3. Zhang, Y., J.-H. Qiu, S. Lin, and D. Wang, "Design of a novel extremely wide band dipole antenna," *Progress In Electromagnetics Research Letters*, Vol. 31, 177–187, 2012.
4. Lin, S., Y. Tian, J. Lu, D. Wu, J.-H. Liu, and H.-J. Zhang, "A UWB printed dipole antenna and ITS radiation characteristic analysis," *Progress In Electromagnetics Research C*, Vol. 31, 83–96, 2012.
5. Lu, J., S. Lin, Y. Tian, L. Jing, M.-Q. Liu, and Z. Zhao, "The simulation and experiment of a UWB printed dipole antenna," *Progress In Electromagnetics Research Letters*, Vol. 36, 21–30, 2013.
6. Yeoh, W. S., K. L. Wong, and W. S. T. Rowe, "Wideband miniaturized half bowtie printed dipole antenna with integrated balun for wireless applications," *IEEE Transactions on Antennas and Propagation*, Vol. 59, No. 1, 339–342, Jan. 2011.
7. Li, D. and J.-F. Mao, "Sierpinskized Koch-like sided multifractal dipole antenna," *Progress In Electromagnetics Research*, Vol. 130, 207–224, 2012.
8. Singh, D. K., D. C. Pande, and A. Bhattacharya, "Selection of ideal feed profile for asymptotic conical dipole fed impulse radiating antenna," *Progress In Electromagnetics Research C*, Vol. 35, 95–109, 2013.
9. Brar, R. S., S. Singhal, and A. K. Singh, "Rotated quadrilateral dipole UWB antenna for wireless communication," *Progress In Electromagnetics Research C*, Vol. 66, 117–128, 2016.
10. Wu, R. and Q. Chu, "Resonator-loaded broadband antenna for LTE700/GSM850/GSM900 base stations," *IEEE Antennas and Wireless Propagation Letters*, Vol. 16, 501–504, 2017.
11. Wen, D., Y. Hao, H. Wang, and H. Zhou, "Design of a wideband antenna with stable omnidirectional radiation pattern using the theory of characteristic modes," *IEEE Transactions on Antennas and Propagation*, Vol. 65, No. 5, 2671–2676, May 2017.
12. Xu, K., F. Liu, L. Peng, W. S. Zhao, L. Ran, and G. Wang, "Multimode and wideband printed loop antenna based on degraded split-ring resonators," *IEEE Access*, Vol. 5, 15561–15570, Jul. 2017.
13. Lu, W. J., W. H. Zhang, K. F. Tong, and H. B. Zhu, "Planar wideband loop-dipole composite antenna," *IEEE Transactions on Antennas and Propagation*, Vol. 62, No. 4, 2275–2279, 2014.
14. Ahdi Rezaeieh, S. and A. M. Abbosh, "Compact planar loop-dipole composite antenna with director for bandwidth enhancement and back radiation suppression," *IEEE Transactions on Antennas and Propagation*, Vol. 64, No. 8, 3723–3728, Aug. 2016.
15. Li, Y., Z. Zhao, J. Liu, and Y.-Z. Yin, "A cavity-backed wideband circularly polarized crossed bowtie dipole antenna with sequentially rotated parasitic elements," *Progress In Electromagnetics Research Letters*, Vol. 79, 1–7, 2018.
16. Li, Y., Q. Feng, and L. Zhou, "Dipole antenna design for portable devices operating in the 5G NR frequency bands," *Progress In Electromagnetics Research Letters*, Vol. 101, 43–48, 2021.
17. Kim, J.-H., M.-G. Jeong, S.-H. Bae, and W.-S. Lee, "A printed fan-shaped meandered dipole antenna with mutual-coupled dual resonance," *IEEE Antennas and Wireless Propagation Letters*, Vol. 16, 3168–3171, 2017.
18. Luk, K.-M. and H. Wong, "A new wideband unidirectional antenna element," *Int. J. of Microwave and Opt. Technology*, Vol. 1, No. 1, 2006.
19. Chen, X., M.-C. Tang, D. Yi, and R. W. Ziolkowski, "Wideband, electrically small, near-field resonant parasitic dipole antenna with stable radiation performance," *IEEE Antennas and Wireless Propagation Letters*, Vol. 19, No. 5, 826–830, May 2020.
20. Lu, W. J., J. Yu, and L. Zhu, "On the multi-resonant antennas: Theory, history and new development," *Int. J. RF Microw. Comp.-Aided Eng.*, Vol. 29, No. 9, e21808, 2019.
21. Mobashsher, A. T. and A. Abbosh, "Slot-loaded folded dipole antenna with wideband and unidirectional performance for L-band applications," *IEEE Antennas and Wireless Propagation Letters*, Vol. 13, 798–801, 2014.
22. Hu, W., X. Liu, S. Gao, L. Wen, Q. Luo, P. Fei, Y. Yin, and Y. Liu, "Compact wideband folded dipole antenna with multi-resonant modes," *IEEE Transactions on Antennas and Propagation*, Vol. 67, No. 11, 6789–6799, Nov. 2019.

23. Shadrokh, S., Y. Q. Yu, F. Jolani, and Z. Chen, "Ultra-compact end-loaded planar dipole antenna for ultra-wideband radar and communication applications," *Electronics Letters*, Vol. 50, No. 21, 1495–1496, Oct. 2014.
24. Shi, Y. and J. Liu, "Investigation of a via-loaded microstrip magnetic dipole antenna with enhanced bandwidth and gain," *IEEE Transactions on Antennas and Propagation*, Vol. 67, No. 7, 4836–4841, Jul. 2019.
25. Li, H. and Y. Li, "Mode compression method for wideband dipole antenna by dual-point capacitive loadings," *IEEE Transactions on Antennas and Propagation*, Vol. 68, No. 8, 6424–6428, Aug. 2020.
26. Luo, Y., Z. N. Chen, and K. Ma, "Enhanced bandwidth and directivity of a dual-mode compressed high-order mode stub-loaded dipole using characteristic mode analysis," *IEEE Transactions on Antennas and Propagation*, Vol. 67, No. 3, 1922–1925, Mar. 2019.
27. Luo, Y., X. Ma, N. Yan, W. An, and K. Ma, "Sidelobe suppression of dual-mode compressed high-order-mode dipole by loading bent stubs," *IEEE Antennas and Wireless Propagation Letters*, Vol. 20, No. 6, 898–902, Jun. 2021.
28. Zhang, W., Y. Li, Z. Zhou, and Z. Zhang, "Dual-mode compression of dipole antenna by loading electrically small loop resonator," *IEEE Transactions on Antennas and Propagation*, Vol. 68, No. 4, 3243–3247, Apr. 2020.
29. Solanki, R., "Compact and broadband uniplanar microstrip antenna for endfire radiation," *Progress In Electromagnetics Research Letters*, Vol. 102, 77–85, 2022.
30. Bindu, K. K., S. Rajbala, K. Girish, and A. K. Singh, "Symmetrically direct coupled stacked broadband microstrip antenna," *IETE Journal of Research*, 2021, doi: 10.1080/03772063.2021.1908856.
31. Sondas, A., M. H. B. Ucar, and Y. E. Erdemli, "Switchable loop-loaded printed dipole antenna with a balun/feed structure," *Microwave and Optical Technology Letters*, Vol. 54, No. 1, 76–79, Jan. 2012.
32. Dassault Systèmes, *CST STUDIO SUITE 2017*, available: https://www.3ds.com/products-services/simulia/products/cst-studio-suite.